JOURNAL OF MATERIALS SCIENCE 26 (1991) 3171–3179

Structural morphology and compaction of nascent high-density polyethylene produced by supported catalysts

J. SCHEIRS*, S. W. BIGGER‡, O. DELATYCKI
Department of Industrial Science, The University of Melbourne, Parkville, 3052, Australia

The morphologies of three nascent high-density polyethylene (HDPE) powders, polymerized in the gas phase by different catalysts, were investigated using scanning electron microscopy (SEM). Silica-supported catalyst systems comprising $TiCl_4/MgCl_2$, *bis*(triphenylsilyl)chromate and *bis*(cyclopentadienyl)chromium were found to produce polymers with globular, nodular and worm-like microstructures, respectively. The topographies of the fluff particles are related to the compaction behaviour of the HDPE powders. Long, worm-like strands that protrude from the particles are capable of forming more extensive entanglements than the shorter, nodular structures. The entanglements are the main cause of agglomeration of the particles during their long-term bulk storage. Furthermore, the rate of thermal oxidation is influenced markedly by the polymer microstructure. The microstructure determines the surface area available for oxygen attack. High-resolution SEM combined with low-temperature plasma etching reveals that the worm-like structures consist of folded-chain lamellae that are coiled around a core of extended chains.

1. Introduction

The gas-phase polymerization of high-density polyethylene (HDPE) is achieved by using supported metal catalysts in a fluidized-bed reactor [1, 2]. The catalysts may be titanium/magnesium or chromium compounds which are reacted on to a high surface area, dehydrated silica substrate. The activity of these catalysts may be increased further by activating the supported transition metal compound with an aluminium alkyl cocatalyst [1]. These highly active catalyst systems enable increased productivity and leave reduced levels of catalyst residue behind in the final polymer [3]. Nascent HDPE produced by organochromium catalysts has a characteristic worm-like structure due to the simultaneous polymerization and crystallization that occurs under shear-field conditions during the gas-phase polymerization. Worm-like morphologies have also been observed in HDPE produced using heterogeneous catalyst systems such as Ziegler–Natta/magnesium oxide [4], titanium/silica [5], chromium oxide/silica [6], vanadium/starch [7] and zirconium/alumina [8, 9].

The polymerization of ethylene on silica-supported catalysts occurs in two stages. Initially, the growing polymer chains encapsulate the silica support particle. Following this, polymer growing within the pores of the silica causes an increase in the internal pressure of the particle, which leads to fracture of the particle and an accelerated polymerization rate due to the increased active surface area. The stage at which the silica support shatters affects the particle size distribution of the polymer [5].

Freshly polymerized HDPE powder (or "fluff") leaves the reactor at approximately 90 °C. The powder may remain at a temperature of 80–85 °C for many days during bulk storage due to its poor heat transfer and very low thermal conductivity. The HDPE resin has a marked tendency to aggregate during long periods of storage and this can cause blockages in plant transfer lines and hoppers. Agglomeration of fluff results from increased granule-to-granule contacts due to the high head pressure in the storage silos. During storage, the bulk density of the fluff increases as finer particles migrate to fill the cavities and interstices between larger particles. As compaction proceeds, the fluff particles undergo elastic deformation followed by plastic flow and this increases the area of contact between the particles.

The mechanical strength of a polymer compact increases as the molecular weight increases [10] and as the particle size of the powder decreases [11, 12]. It has also been established that polymeric powders having irregular, spongy particles form stronger compacts than those consisting of spherical, dense particles [13–15]. However, ultrahigh molecular weight polyethylene (UHMWPE) compacts well despite having relatively large particles of regular shape. This behaviour was attributed originally to its high

* Author to whom all correspondence should be addressed.
‡ *Present address*: Department of Physical Chemistry, The University of Melbourne, Parkville, 3052, Australia.

0022–2461/91 $03.00 + .12

molecular weight [10] but, more recently, its fibrous surface morphology has been used to explain this phenomenon [16]. Other studies of UHMWPE have confirmed that surface morphology and particle size can influence the strength of its powder compacts [17, 18].

Nascent HDPE fluff is very susceptible to thermo-oxidative degradation because it contains no anti-oxidants and usually consists of small particles of large surface area [19]. The long-term storage of HDPE fluff at elevated temperatures leads to the formation of hydroperoxide groups followed by a reduced molecular weight of the polymer due to oxidative chain scission processes [20]. During subsequent compounding, cross-linking occurs and causes a decrease in the melt flow index (MFI) of the polymer. In addition, hydroperoxide groups may decompose to form carbonyl and other oxygenated groups that can act as photosensitizers [21, 22]. The storage stability of HDPE fluff can be improved by blanketing it with an inert gas [19] or by adding a phenolic stabilizer during polymerization [23].

The etching of nascent HDPE using reagents such as fuming nitric acid has been used to elucidate its lamellar morphology [24, 25]. The chemical etching of polymers also provides valuable structural information relating to the regions that are affected by thermal oxidation. However, the reprecipitation of etched material may create artefacts on the treated surface [26]. In contrast, the method of low-temperature plasma etching has been used successfully to remove preferentially the amorphous region from HDPE without the deposition of debris [27–32].

This present work investigated the relationship between the compaction behaviour, morphology and oxidative stability of nascent HDPE during storage. Polymers were produced using three different catalyst systems and the morphologies of their nascent fluff particles were characterized using scanning electron microscopy (SEM). Low-temperature plasma etching was used to reveal the orientation of the lamellae which comprise the worm-like microstructures.

3. Experimental procedure

3.1. Materials

Three types of HDPE were produced by gas-phase polymerization in a fluidized-bed reactor in the temperature range of 90–110 °C using transition metal catalysts supported on dehydrated silica. Density and MFI values of the samples were measured in accordance with ASTM Methods D792-66 and D1238-7, respectively. The physical properties of the HDPE materials are listed in Table I.

HDPE(1) is a copolymer with 1-hexene and was produced on a supported $TiCl_4/MgCl_2$ catalyst [33–35]. HDPE(2) is a copolymer with 1-butene and was made on a supported *bis*(triphenylsilyl)chromate catalyst [36–38]. HDPE(3) was polymerized using a supported *bis*(cyclopentadienyl)chromium catalyst [39–42]. The HDPE(1) and HDPE(2) catalysts were reduced chemically to an active state using $Al(C_2H_5)_3$ and $Al(C_2H_5)_2OCH_2CH_3$ cocatalysts, respectively. The highly active catalyst used for HDPE(3) required no addition of cocatalyst.

A 50 g sample of each HDPE material was pyrolysed in a muffle furnace for 2 h at 400 °C in order to determine its ash content (see Table I). Samples of HDPE(3) fluff were etched for SEM examination using a low-temperature argon plasma at 0.05 torr (1 torr = 1.333×10^2 Pa) for 5 h.

3.2. Compaction and oxidation methods

The bulk densities of the HDPE samples were measured in accordance with ASTM D-1895 (Method B). Samples of fluff were fractionated by dry sieving, using BSS screens, to obtain narrow particle size distributions [43]. The fractions were compacted in a 21 mm diameter stainless steel compression die. A barrel charge of 4.5 g and a loading of 0.21 MPa, at a rate of 0.07 MPa s^{-1}, were used in each case. The dwell time was 180 s and all tests were performed at room temperature. The compressive strength of each compacted stub was determined using a universal testing machine at a crosshead speed of 20 mm min^{-1}.

Oxidized HDPE samples were produced by storing the virgin powder in an air-circulating oven at 80 °C for up to 14 days. The rate of oxidation was assessed by measuring the MFI of each material as a function of ageing time. An extensively oxidized sample for SEM examination was produced by storing HDPE(2) powder in air at 80 °C for 28 days.

3.3. Scanning electron microscopy

The nascent HDPE fluff was examined by SEM. Samples were mounted on aluminium stubs with conductive cement and, to prevent charging, were sputter-coated with a 30 nm layer of gold in a vacuum

TABLE I Physical characteristics of the polymers

Sample	M_w (10^{-3} a.m.u.)	Polydispersity M_w/M_n	Density (g cm^{-3})	MFI[a]	Ash content (p.p.m.)
HDPE(1)	185	5.3	0.9340	4.3[b]	450
HDPE(2)	338	22.8	0.9520	1.0[c]	250
HDPE(3)	276	8.2	0.9605	0.9[b]	200

[a] g/10 min at 190 °C.
[b] Determined using 2.16 kg mass.
[c] Determined using 5.0 kg mass.
[d] M_w and polydispersity determined by gel permeation chromatography.

sputterer. Electron micrographs were taken on an Hitachi Model S570 scanning electron microscope equipped with a lanthanum hexaboride (LaB_6) crystal electron source instead of the usual tungsten filament. This source has a greater electron efficiency than conventional tungsten sources and was operated at an accelerating voltage of 5 kV to reduce electron beam damage of the delicate microstructure of the fluff.

4. Results and discussion

4.1. HDPE powder compaction

The tendency of each polymer powder to agglomerate, as a function of its surface morphology and particle size, was tested by compacting it and measuring its compressive strength. Fig. 1 shows the compressive strength of compacts that were produced from different particle size fractions of the HDPE(2) and HDPE(3) materials. The compressive strength of the samples correlates with their degree of compactibility and decreases as the average particle size increases. All particle size fractions of HDPE(1) have no measurable compressive strength under the compaction conditions used. The compressed HDPE(1) fluff could be poured from the die with no apparent adhesion between the particles. The HDPE(2) material could be compacted to produce samples of moderate compressive strength except for its coarsest fraction (> 850 μm) which could not be compacted into stable test samples. The HDPE(3) fluff compacted to produce billets that were up to ten times stronger than the HDPE(2) compacts.

Fig. 2a is a micrograph of a typical HDPE(1) fluff particle showing its characteristic spherical shape. The particles of this polymer tend to replicate the shape of the parent silica support [33, 44]. The surface undulations of the HDPE(1) particles inhibit their close packing. These features, together with voids that result from particle bridging, account for the low bulk density (0.43 $g\,cm^{-3}$) of HDPE(1). In contrast, HDPE(2) and HDPE(3) have irregular particle shapes (see Fig. 2b and c) and their bulk densities are, therefore, relatively high (0.51 and 0.55 $g\,cm^{-3}$, respectively).

Fig. 3 is a high magnification micrograph of an HDPE(1) fluff particle. At this magnification the surface is rather featureless although it does show small cracks bridged by microfibrils. Figs 4 and 5 are micro-

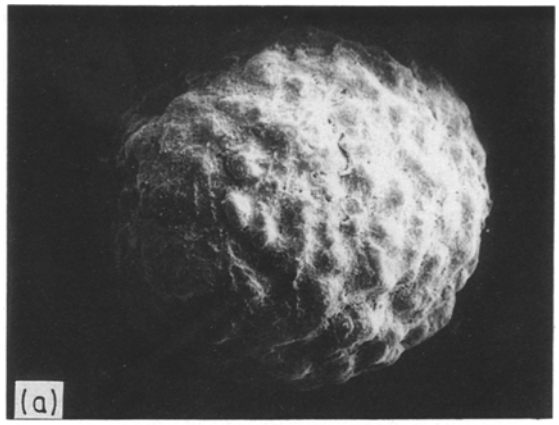

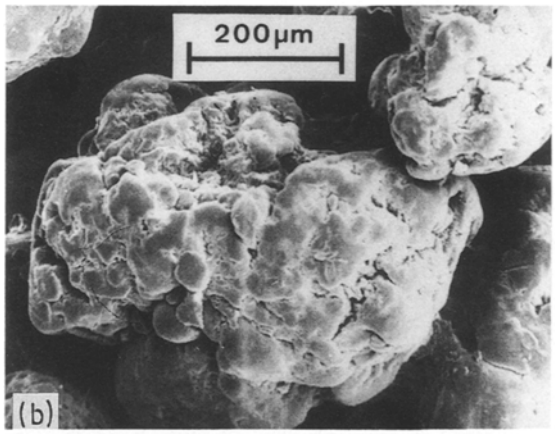

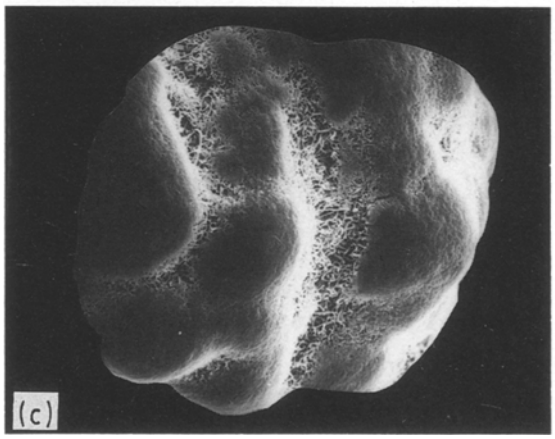

Figure 2 Micrographs of (a) HDPE(1), (b) HDPE(2) and (c) HDPE(3) showing the typical shapes of their fluff particles.

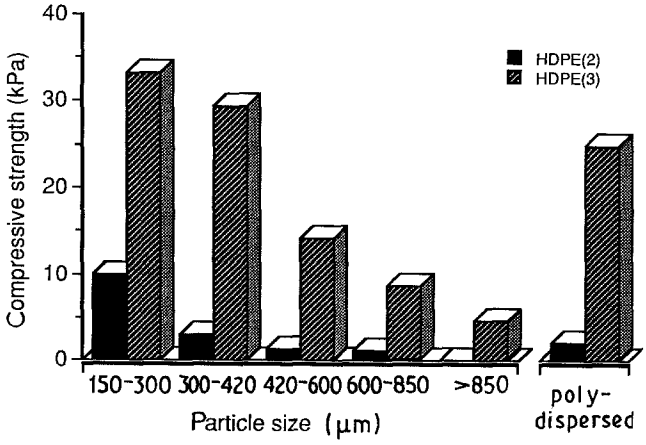

Figure 1 Compressive strength versus particle size fractions of HDPE(2) and HDPE(3) compacts.

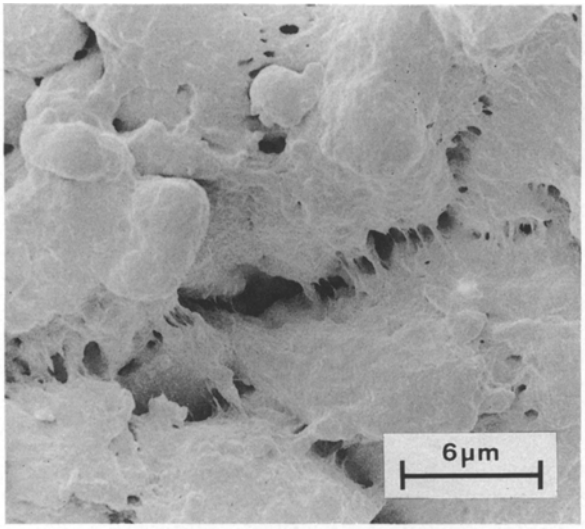

Figure 3 Micrograph of the surface of an HDPE(1) fluff particle.

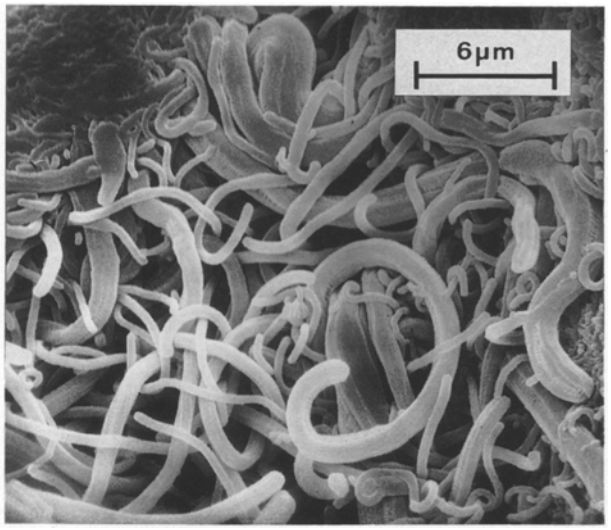

Figure 5 Micrograph of the surface of an HDPE(3) fluff particle

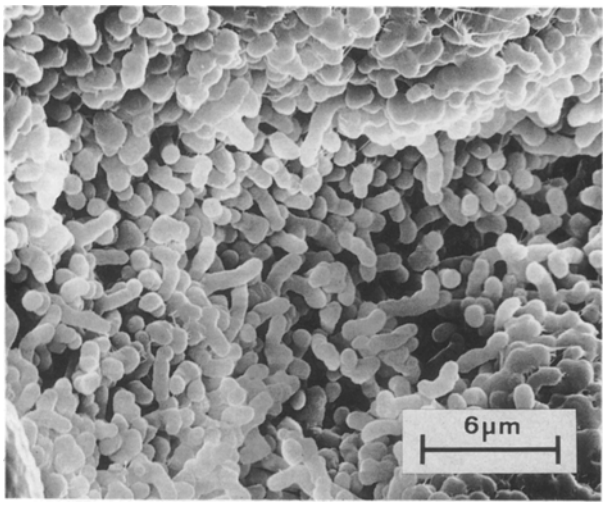

Figure 4 Micrograph of the surface of an HDPE(2) fluff particle.

graphs of the HDPE(2) and HDPE(3) materials, respectively. All of these micrographs are of the same magnification for comparative purposes. The micrograph of the HDPE(2) material indicates a nodular microstructure in which the nodules are approximately 0.5 μm in diameter. On the other hand, the HDPE(3) micrograph shows prolific, tangled, worm-like structures that are about 1,0 μm in diameter and up to 10 μm in length.

The degree of compaction of the three samples is related to the propensity of their microstructures to form entanglements. The intertwining of the longer, worm-like structures of HDPE(3) forms particle agglomerates, whereas the nodular structure of HDPE(2) is not as effective in forming extensive entanglements. In the coarser HDPE(2) fractions, the ratio of the size of the nodule to the total fluff particle size is small and thus the entanglement effectiveness is very low. This may account for the decrease in the compressive strength as the sample fractions become coarser (see Fig. 1). The behaviour of HDPE(3) can also be explained in terms of the entanglements of its worm-like structures. Furthermore, the irregularity of the HDPE(2) and HDPE(3) particles may contribu to their mechanical interlocking during compressi [43].

Particles of HDPE(2) and HDPE(3) are mo porous than those of HDPE(1) (see Figs 3–5) and th is consistent with the fact that both of these polyme are easily compacted whereas HDPE(1) is quite u yielding. It has been found that relatively poro particles allow some yielding to occur on compacti thus increasing the surface area of contact betwe them [13].

4.2. Polymer microstructure

4.2.1. Structural morphology

Fig. 6 is a high resolution micrograph showing t end of an HDPE(3) worm-like strand. Fig. 7 shows longitudinal portion of the strand and highlights underlying structure. The presence of overlaid pol mer filaments provides evidence to support the fa that epitaxial crystallization has occurred during pol merization. The micrograph also shows that t lamellar overgrowths are oriented perpendicular the fibrillar axis due to the stresses imposed duri crystallization, whereas the core consists of extend chains that are aligned parallel to the direction of t shear field. The folded-chain lamellae are laid down the preformed, extended chain and this process governed by thermodynamic and kinetic facto [45–47]. Similar morphology has been observed nascent HDPE that was polymerized using oth transition metal catalysts [48–50]. Electron diffra tion studies [51, 52] confirm that the long axis of t polymer chain overgrowths is parallel to the grow direction of the worm-like structures.

The microstructure of HDPE(3), which was etch in a low-temperature plasma to remove its amorpho regions, is shown in Fig. 8. The crystalline, skelet remains of the worm-like strands show regular lam lar units. This morphology arises from the simulta eous polymerization and crystallization that occu under shear-field conditions. These conditions are al responsible for the widely reported "shish kebal

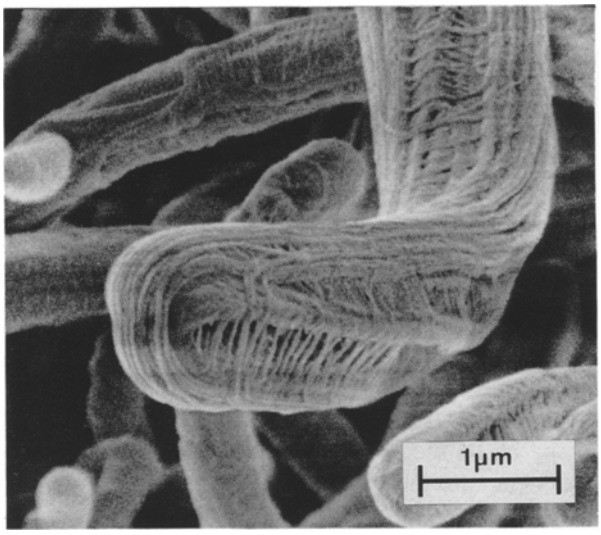

Figure 6 Micrograph of the end of an HDPE(3) worm-like strand.

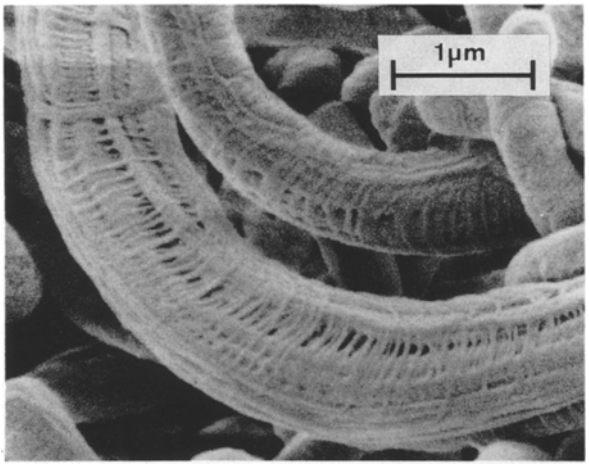

Figure 7 Micrograph showing a longitudinal portion of an HDPE(3) worm-like strand.

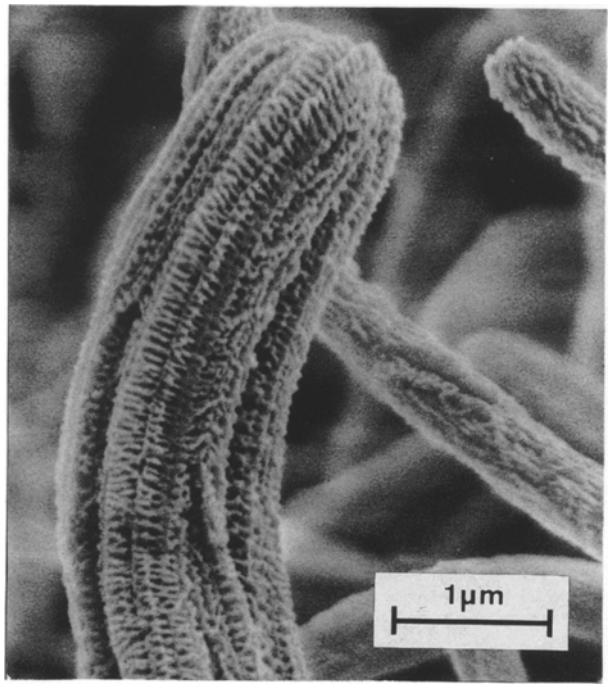

Figure 8 Micrograph of plasma-etched HDPE(3).

morphology [53] which is obtained from the stirred solution polymerization of polyethylene. It has been well established that the "shish kebab" structure is composed of extended chains with distinct, regularly-spaced, folded-chain domains [54].

The microstructure of nascent HDPE(3) shows a dual morphology consisting of a crystalline, extended-chain core enveloped by chain-folded lamellae. In this respect the morphology resembles that of the "shish kebab" model. However, unlike the "shish kebab" structure, the folded chain lamellae in HDPE(3) are randomly wound around the core to produce a woven or "net-like" arrangement. This "cross-hatched" texture probably results from the multiple deposition of lamellar material that occurs during polymerization. The microstructure of plasma-etched HDPE(3) is similar to that of ion-etched, drawn HDPE in which the lamellae are arranged perpendicular to the direction of drawing [55, 56]. It is likely, therefore, that the worm-like structures of HDPE(3) are oriented parallel to their growth direction.

The extended and folded-chain regions have different coefficients of thermal expansion which causes the strands to move as the temperature changes. Such movement is observed during SEM examination where prolonged electron beam exposure heats the sample. In practice, this motion may contribute to the degree of entanglement between the strands that occurs during their cooling in long-term storage.

4.2.2. Growth of worm-like structures

The large differences in the microstructures of the samples are related to the activities of their catalyst systems as well as to the distribution of each catalyst on its silica support. The HDPE(1) catalyst does not interact chemically with its support and thus produces a random spatial orientation of surface active sites. The surface undulations on the HDPE(1) fluff particles consist of unevenly distributed crystalline arrays. The HDPE(2) and HDPE(3) catalysts have many active sites that are located in close proximity to each other and are bound chemically to the catalyst support. This arrangement of the catalytic sites is responsible for the nodular and worm-like microstructures present in these polymers. The formation of nodules in HDPE(2) is due to its catalyst producing polymerization conditions being more moderate than those in the HDPE(3) system. This is consistent with previous studies [57] which found that at a low polymerization rate a globular morphology is formed while nodular and worm-like morphologies are formed at high polymerization rates. The nodules in HDPE(2) protrude from the surface to almost the same level and this suggests that their rate of growth is similar (see Fig. 4).

The microstructure of nascent HDPE, produced in hexane solution at 80 °C using silica-supported *bis*(cyclopentadienyl)chromium, is shown in a recent publication [58]. The structure is composed of microglobules of approximately 0.7 μm diameter which contrasts with the worm-like strands formed in HDPE(3). These marked structural variations may be attributable to the different polymerization media used or,

alternatively, to differences in the calcining treatment of the silica support prior to catalyst deposition. A globular morphology has been obtained using an unsupported $TiCl_4/Al(C_2H_5)_3$ catalyst system but a worm-like structure resulted when this catalyst was supported on a magnesium oxide carrier [4]. Furthermore, the slurry-phase polymerization of HDPE using a $TiCl_4/MgCl_2/SiO_2$ catalyst was found to produce a globular texture due to the relatively low efficiency of this catalyst system. However, a worm-like morphology can be produced by adding an aluminium alkyl cocatalyst which increases the overall catalyst efficiency [59].

It is believed that the worm-like structures in HDPE(3) originate from regions where there is a concentration of active sites. The lateral growth of these structures is restricted by surrounding strands and thus growth proceeds in a direction perpendicular to the surface of the substrate until chain termination occurs. At this point the internal stresses that operate during polymerization and crystallization are relaxed and the longer strands adopt a twisted and tangled conformation.

Fig. 9 is a micrograph of HDPE(3) showing many of the worm-like strands. It is interesting to note the presence of several branched structures. This suggests that active catalyst sites are sufficiently mobile to initiate the growth of the strands at positions far removed from the parent silica support. This behaviour is consistent with the "tip-growth" model of nascent polyethylene [60, 61] in which active catalyst particles break away from the support and reside in the vicinity of the growth front. These mobile catalyst particles may be responsible for the initiation of branches in the worm-like structure. It is essential, however, that some of the support material remains bound to the catalyst so that catalytic activity does not diminish due to the mutual destruction of active sites.

The "base-growth" model [47, 62] has also been proposed to explain the worm-like texture of nascent HDPE. In this model active sites remain fixed to the parent support and new polymer is formed at the base of the growing filament thereby displacing the existing polymer from the surface of the substrate. It is unlikely that this model applies to the HDPE(3) system because the model does not explain the observed occurrence of filament branching. Furthermore, if the branches were formed by the fusion of adjacent base-growing filaments then the branch ends would be tapered or drawn during their detachment from the catalyst surface. This behaviour cannot be inferred from the micrographs presented in this paper. In addition, the examination of nascent zirconium-catalysed HDPE using transmission electron microscopy has confirmed the presence of catalyst support fragments at the tips of the filaments [63].

4.2.3. Cobweb formation

Fig. 10 is a micrograph showing the interconnecting fibrils or the "cobweb" structure of HDPE(2). The *bis*(triphenylsilyl)chromate catalyst system causes an initial induction period which precedes the steady-state polymerization. In the initial stage a crust of polymer slowly encapsulates the silica support particle [64]. This is followed by an increase in the polymerization rate within the particle which causes the polymer crust to crack and separate. In addition, the fragmentation of the silica support exposes many new active sites which promote polymerization and this further increases the pressure within the particle. As the crust disintegrates segments remain connected by a network of drawn fibrils. The fibrils extend over a distance of about 20 μm and have a diameter of approximately 0.1 μm.

Similarly, stretched fibrillar structures are observed on the surfaces of the HDPE(1) particles (see Fig. 3).

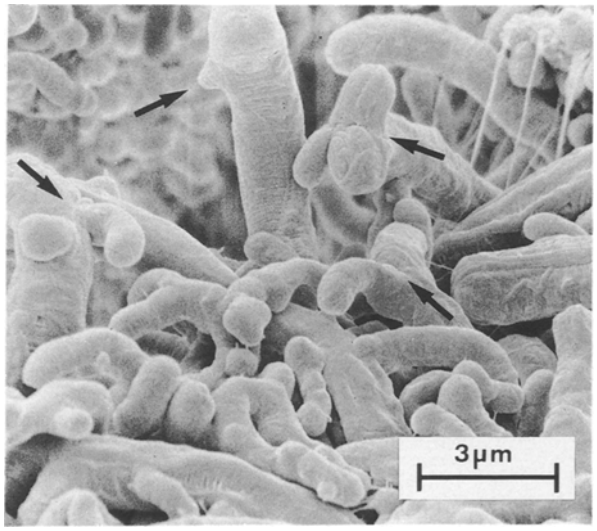

Figure 9 Micrograph of an HDPE(3) fluff particle showing branched, worm-like structures.

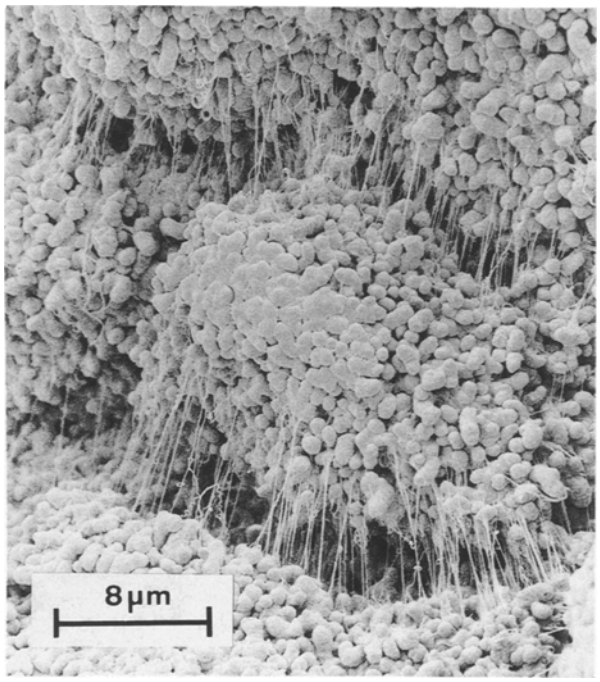

Figure 10 Micrograph showing the cobweb structure on the surface of an HDPE(2) fluff particle.

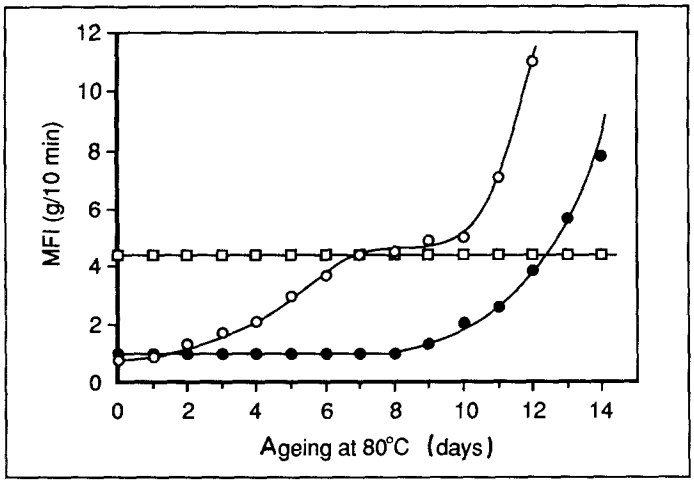

Figure 11 Plots of MFI versus ageing time at 80 °C for (□) HDPE(1), (●) HDPE(2) and (○) HDPE(3).

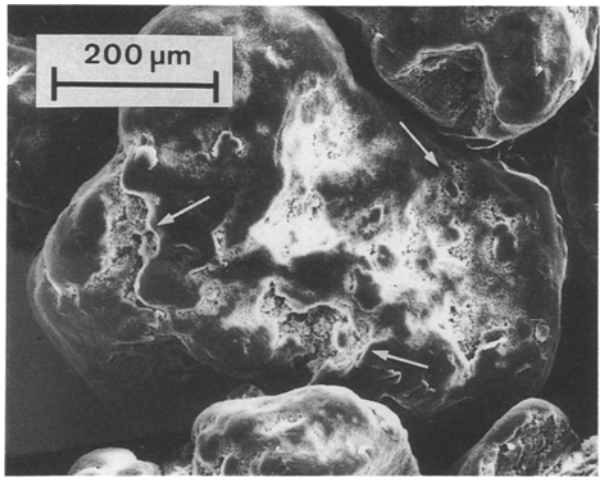

Figure 12 Micrograph of an HDPE(2) fluff particle which was oxidized in air at 80 °C for 28 days. The arrows indicate the embrittled regions.

However, these fibrils are not as extensively drawn and are fewer in number than those in the HDPE(2) polymer. This may be due to the lower activity and more random spatial distribution of the active sites in the HDPE(1) catalyst system. The presence of interconnected arrays of drawn fibrils between the nodules in nascent HDPE has been noted elsewhere [52, 64–68]. Cobweb morphology usually results from polymerizations that have a slow initial stage prior to steady-state conditions. The polymerization of HDPE using a $TiCl_4/MgCl_2$ catalyst with an $Al(C_2H_5)Cl$ cocatalyst is a recently reported example of a system that exhibits this sort of rate profile and as such produces a polymer which has a cobweb morphology [59].

4.3. Thermal oxidation

Fig. 11 shows the variation in MFI with ageing time in air at 80 °C for the three HDPE materials. The HDPE(1) sample is the most resistant to thermal oxidation as its MFI value remains constant over the test period whereas for both HDPE(2) and HDPE(3) the MFI varies with ageing time. After an initial period of 8 days during which almost no change is observed, the MFI of HDPE(2) increases rapidly. The HDPE(3) sample shows the fastest rate of oxidation, which is indicated by the almost instantaneous increase in MFI upon exposure to heat.

The HDPE(2) has a higher degree of branching and unsaturation than HDPE(3), as well as having a greater concentration of catalyst residue (see Table I). However, Fig. 11 shows that HDPE(2) oxidizes more slowly than HDPE(3). This seemingly anomalous behaviour can be explained by the fact that HDPE(3) has a much higher surface area available for oxidation (see Fig. 4). Furthermore, HDPE(1) does not have a nodular or worm-like microstructure and, therefore, has the lowest surface area of the three materials. This accounts for its greater oxidative stability compared with either HDPE(2) or HDPE(3), despite its relatively high level of catalyst residue (see Table I).

Fig. 12 shows micrographs of HDPE(2) which were taken after 28 days of thermal treatment. Oxidative chain scission causes the surface of each polymer particle to embrittle. A localized density increase accompanies this process and causes the particle surface to crack and flake. This, in turn, exposes the inner regions of the particle and promotes further oxidation as more surface area is revealed. It is expected that the HDPE(1) material will show similar behaviour over a sufficiently long time period.

5. Conclusions

The microstructure of nascent HDPE is determined largely by the rate of polymerization which, in turn, depends on the nature and efficiency of the catalyst system used in its production. In particular, the specific chemical interactions that occur between chromium-based catalysts and their silica supports can produce characteristic nodular and worm-like morphologies. The resultant microstructure of the polymer significantly affects both its degree of compaction and its rate of oxidation during long-term storage. The degree of compaction is related to the extent of the entanglements between the microstructures that protrude from the fluff particles. Furthermore, the rate of oxidation of the polymer is influenced by the surface area that is susceptible to direct oxygen attack.

An interesting morphological variation of the familiar "shish kebab" structure has been revealed in this study. The HDPE prepared using the *bis*(cyclopentadienyl)chromium catalyst, has a unique microstructure comprised of folded chain lamellae that are wound around a core of extended chains to produce a "net-like" or "cross-hatched" arrangement. The oriented nature of these worm-like structures can be elucidated using the technique of low-temperature plasma etching, which has the advantage of minimizing artefact formation. The presence of branched, worm-like strands in this material is consistent with the "tip-growth" polymerization model.

Acknowledgements

The authors thank Commercial Polymers Australia Limited for financial support, Mr J. Nailon, Department of Botany, Monash University, for his help with the SEM work, Drs G. Hawthorne and H. Griesser, CSIRO Division of Chemicals and Polymers, for their assistance with GPC measurements and plasma etching, Mr G. J. Pratt, Department of Industrial Science, The University of Melbourne, for reading the manuscript.

References

1. F. J. KAROL, in "Encyclopedia of Polymer Science and Technology-Supplement", Vol. 1 (Wiley, New York, 1976) p. 120.
2. F. J. KAROL, B. E. WAGNER, I. J. LEVINE, G. L. GOEKE and A. NOSHAY, in "Advances in Polyolefins", edited by R. B. Seymour and T. Cheng (Plenum Press, New York, 1987) p. 337.
3. Anon., *Chem. Engng* November (1973) 72.
4. A. A. BAULIN, A. Ya. GOLDMAN, A. B. FREIDIN, V. I. SELIKHOVA, Yu. A. ZUBOV and S. S. IVANCHEV, *Int. Polym. Sci. Technol.* **9** (1982) 100.
5. A. MUNOZ-ESCALONA, J. G. HERNADEZ and J. A. GALLARDO, *J. Appl. Polym. Sci.* **29** (1984) 1187.
6. T. DAVIDSON, *J. Polym. Sci. B* **8** (1970) 855.
7. H. D. CHANZY, J. F. REVOL, R. H. MARCHESSAULT and A. LAMANDA, *Kolloid Z. Z. Polym.* **251** (1973) 563.
8. D. G. H. BALLARD, *J. Polym. Sci. Polym. Chem. Ed.* **13** (1975) 2191.
9. A. AKAR, N. C. BILLINGHAM, P. D. CALVERT, *Polymer* **24** (1983) 889.
10. T. MAEDA and S. MATSUOKA, *J. Faculty Engng Univ. Tokyo* **33** (1975) 191.
11. G. S. JAYARAMAN, J. F. WALLACE, P. H. GEIL and E. BAER, *Polym. Engng Sci.* **16** (1976) 529.
12. D. M. BIGG, *ibid.* **17** (1977) 691.
13. D. M. GALE, *J. Appl. Polym. Sci.* **22** (1978) 1955.
14. R. J. CRAWFORD and D. PAUL, *J. Mater. Sci.* **14** (1979) 2693.
15. *Idem, ibid.* **17** (1982) 2267.
16. R. W. TRUSS, K. S. HAN, J. F. WALLACE and P. H. GEIL, *Polym. Engng Sci.* **20** (1980) 747.
17. K. S. HAN, J. F. WALLACE, R. W. TRUSS and P. H. GEIL, *J. Macromol. Sci. Phys.* **B 19** (1981) 313.
18. A. SIEGMANN, I. RAITER, M. NARKIS and P. EYERER, *J. Mater. Sci.* **21** (1986) 1180.
19. P. P. KLEMCHUK and P. L. HORNG, *Polym. Degrad. Stab.* **7** (1984) 131.
20. S. AL-MALAIKA and G. SCOTT, in "Degradation and Stabilization of Polyolefins", edited by N. Allen (Applied Science, London, 1983) p. 247.
21. G. V. HUTSON and G. SCOTT, *Chem. Ind* (1972) 725.
22. *Idem, Eur. Polym. J.* **10** (1974) 45.
23. G. L. GOEKE, A. D. HAMER and F. J. KAROL, Eur. Pat. Appl. 3836 (1979).
24. A. MUNOZ-ESCALONA and A. PARADA, *Polymer* **20** (1979) 859.
25. *Idem, J. Crystal. Growth* **48** (1980) 250.
26. M. M. WINRAM, D. T. GRUBB and A. KELLER, *J. Mater. Sci.* **13** (1978) 791.
27. L. I. BEZRUK and Yu. S. LIPATOV, in "International Symposium on Macromolecules", Vol. 2, Leiden, The Netherlands (IUPAC, 1970) p. 823.
28. L. I. BEZRUK and Yu. S. LIPATOV, *Plast. Massy.* **7** (1973) 70.
29. J. R. HOLLAHAN, in "Techniques and Applications of Plasma Chemistry" (Wiley, New York, 1974) p. 229.
30. J. S. MIJOVIC and J. A. KOUTSKY, *Polym. Plast. Technol. Engng* **9** (1977) 139.
31. J. FRIEDRICH, J. GAHDE and M. POHL, *Acta Polym.* **31** (1981) 310.
32. L. C. SAWYER and D. T. GRUBB, in "Polymer Microscopy" (Chapman and Hall, London, 1987) p. 112.
33. Eur. Pat. 4651 (1979).
34. G. L. GOEKE, B. E. WAGNER and F. J. KAROL, US Pat. 4 302 565 (1981).
35. F. J. KAROL, G. L. GOEKE, B. E. WAGNER, W. A. FRASER, R. J. JORGENSEN and N. FRIIS, US Pat. 4 302 566 (1981).
36. W. L. CARRICK, G. L. KARAPINKA and R. J. TURBETT, US Pat. 3 324 095 (1967).
37. L. M. BAKER and W. L. CARRICK, US Pat. 3 324 101 (1967).
38. W. L. CARRICK, R. J. TURBETT, F. J. KAROL, G. L. KARAPINKA, A. S. FOX and R. N. JOHNSON, *J. Polym. Sci. A1* **10** (1972) 2609.
39. F. J. KAROL, G. L. KARAPINKA, C. WU, A. W. DOW, R. N. JOHNSON and W. L. CARRICK, *ibid.* **10** (1972) 2621.
40. F. J. KAROL, G. L. BROWN and J. M. DAVISON, *ibid.* **11** (1973) 413.
41. G. L. KARAPINKA, US Pat. 3 709 853 (1973).
42. F. J. KAROL and G. L. KARAPINKA, US Pat. 3 709 954 (1973).
43. G. W. HALLDIN and I. L. KAMEL, *Polym. Engng Sci.* **17** (1977) 21.
44. P. MACKIE, M. N. BERGER, B. M. GRIEVESON and D. LAWSON, *J. Polym. Sci. B* **5** (1967) 493.
45. T. DAVIDSON, *Polym. Prepr. (ACS Div. Polym. Chem.)* **12** (1971) 478.
46. A. KELLER and F. M. WILLMOUTH, *J. Macromol. Sci. Phys. B* **6** (1972) 493.
47. J. WRISTERS, *J. Polym. Sci., Polym. Phys. Ed.* **11** (1973) 1601.
48. H. D.CHANZY, A. DAY and R. H. MARCHESSAULT, *Polymer* **8** (1967) 567.
49. A. G. WIKJORD and R. St. JOHN MANLEY, *J. Macromol. Sci. Phys. B* **2** (1968) 501.
50. A. KELLER and F. M. WILLMOUTH, *Makromol. Chem.* **121** (1969) 42.
51. D. G. H. BALLARD, E. JONES, R. J. WYATT, R. T. MURRAY and P. A. ROBINSON, *Polymer* **15** (1974) 169.
52. R. T. MURRAY, in "Characterization of Catalysts" (Wiley, New York, 1980) p. 105.
53. F. M. WILLMOUTH, A. KELLER, I. M. WARD and T. WILLIAMS, *J. Polym. Sci. A2* **6** (1968) 1627.
54. R. G. CRYSTAL and J. H. SOUTHERN, *ibid.* **9** (1971) 1641.
55. T. TAGAWA and J. MORI, *J. Electron Microsc.* **27** (1978) 267.
56. M. KOJIMA and H. SATAKE, *J. Polym. Sci., Polym. Phys. Ed.* **20** (1982) 2153.
57. A. MUNOZ-ESCALONA, C. VILLAMIZAR and P. FRIAS, *Polym. Sci. Tech. (Struct.-Prop. Relat. Polym. Solids)* **22** (1983) 95.
58. N. V. SEMIKOLENOVA, G. A. NESTEROV, V. A. ZAKHAROV, G. N. KRYUKOVA, V. P. IVANOV and G. I. GOLDENBERG, *Makromol. Chem.* **189** (1988) 1739.
59. I. KIM and S. I. WOO, *Polym. J.* **21** (1989) 697.

60. H. D. CHANZY, E. BONJOUR and R. H. MARCHESSAULT, *Colloid Polym. Sci.* **252** (1974) 8.
61. D. G. H. BALLARD, E. JONES, A. J. P. PIOLI, P. A. ROBINSON and R. J. WYATT, Brit. Pat. 1 314 828 (1973).
62. C. W. HOCK, *J. Polym. Sci. A1* **4** (1966) 3055.
63. D. G. H. BALLARD, P. A. HOLMES and P. J. SENIOR, in "Recent Advances in Mechanistic and Synthetic Aspects of Polymerization", NATO ASI Ser., Ser. C. (Reidel, New York, 1987) p. 293.
64. R. L. GRAFF, G. KORTLEVE and C. G. VONK, *J. Polym. Sci. B* **8** (1970) 735.
65. H. D. CHANZY, B. FISA and R. H. MARCHESSAULT, *Crit. Rev. Macromol. Sci.* **1** (1973) 315.
66. M. MIHAILOV, L. MINKOVA, E. NEDKOV and R. KIRCHEVA, *Makromol. Chem.* **180** (1979) 2351.
67. A. MUNOZ-ESCALONA, J. G. HERNANDEZ, J. A. GALLARDO and A. SUSTIC, in "Advances in Polyolefins", edited by R. B. Seymour and T. Cheng (Plenum Press, New York, 1987) p. 179.
68. L. MINKOVA, M. VELIKOVA and D. DAMYANOV, *Eur. Polym. J.* **24** (1988) 661.

Received 10 January
and accepted 4 September 1990